Journal of Catalysis **185,** 58–72 (1999)
Article ID jcat.1999.2494, available online at http://www.idealibrary.com on IDEAL®

Aging and Structure/Activity Characteristics of CR–ZSM-5 Catalysts during Exposure to Chlorinated VOCs

Ramesh Rachapudi, Prashant S. Chintawar, and Howard L. Greene[1]

Department of Chemical Engineering, The University of Akron, Akron, Ohio 44325-3906

Received September 8, 1998; revised January 4, 1999; accepted March 18, 1999

This study investigates the aging and partial deactivation process for four chromium exchanged ZSM-5 catalysts during oxidative destruction of 1% vinyl chloride or trichloroethylene, each in humid (1.35% water) air at 500°C. After 51 h on stream under these harsh conditions, all catalysts are found to undergo partial loss of exchanged chromium, which correlates with the chlorine content of the chlorinated VOC (CVOC) feed molecule. Conversely, changes in catalytic activity are not entirely correlated with residual chromium levels in the zeolite, suggesting that the chromium cation location is also important. A deactivation pathway is proposed involving slow generation of volatile CrO_2Cl_2 to explain the process of cation migration and loss. These results are utilized to derive relationships between catalyst structure (cation site locations, accessibilities, and framework bond strengths) and catalytic properties (activity, selectivity, and site stability). The analysis shows that Cr cations, which are closely associated with a maximum number of zeolite framework oxygen atoms, are most resistant to migration or loss from the catalyst during CVOC oxidation. Chromium sites (S_{II}, S_{III}) within the straight channels or near channel intersections are found to be most active, but are also most prone to migration and/or loss. This enhanced activity is believed to occur because of the high accessibility of S_{II} and S_{III} sites to incoming CVOC molecules. Rapid loss of chromium from these sites is believed to be due to their weak association with the zeolite framework. Conversely, chromium sites (S_I, S_{IV}) located in the sinusoidal channels are determined to be less active, but more persistent during deactivation because of their increased coordination with zeolite framework atoms and reduced accessibility to incoming CVOC molecules.

INTRODUCTION

Catalyst Activity, Selectivity, and Aging

Earlier investigations from this laboratory (1, 2) have shown the capability of chromium exchanged Y- and ZSM-5-zeolite catalysts (Cr–Y and Cr–ZSM-5) for the oxidative destruction of many CVOCs. These catalysts, especially Cr–Y, appeared to undergo modest deactivation when exposed to CVOCs for an extended period of time (3–5). Rachapudi (3) studied the deactivation of chromium-containing (exchanged or impregnated) Y-zeolite catalysts during the oxidative destruction of ~1200 ppm TCE in humid air at elevated temperature (600°C). It was reported that the irreversible deactivation was caused primarily by the partial loss of catalytically active component, i.e., chromium. However, the Y-zeolitic support also underwent partial structural collapse apparently due to its interaction with corrosive reaction products such as HCl and Cl_2. At lower temperatures (especially 175–250°C), Chatterjee *et al.* (4) reported the reversible deactivation of cobalt and chromium containing Y-zeolite catalysts due to coking during the oxidative destruction of ~1100 ppm TCE, dichloromethane, or carbon tetrachloride in humid air.

Karmakar and Greene (5) studied the deactivation of H–Y and Cr–Y catalysts during oxidative destruction of 1500–2000 ppm CFC11 (CCl_3F) and CFC12 (CCl_2F_2) in dry air at 300°C. Although both the catalysts underwent deactivation after 7 h on stream, a significantly higher degree of deactivation was observed for the H–Y catalyst than for the Cr–Y catalyst. The authors attributed the improved stability of the Cr–Y catalyst to the greater stability of the zeolitic matrix, due to the multivalency of exchanged chromium cations.

The deactivation of metal or metal oxide supported catalysts during the oxidative destruction of CVOCs has also been widely studied. Spivey and Butt (6) have given an excellent review, which covers the work until 1991. The authors state that CVOCs are generally poisons for supported noble metal catalysts and can interact with the noble metal or the support in a reversible or irreversible fashion. It is concluded that HCl or Cl_2 produced by the oxidation reaction itself may be the catalyst poison. On metal oxides, the authors state that chlorine may form volatile metal-containing compounds leading to the loss of the catalytic agent.

Recently, Agarwal and coworkers (7) investigated the long-term stability of commercial Cr_2O_3/Al_2O_3 catalyst during the oxidative destruction of C_1 and C_2 chlorinated hydrocarbons. A progressive loss in the catalytic activity was

[1] To whom correspondence should be addressed at Department of Chemical Engineering, Case Western Reserve University, Cleveland, OH 44106-7217. Fax: (216) 368-3016. E-mail: hlg3@po.cwru.edu.

0021-9517/99 $30.00

observed in the catalyst bed during 153 days on stream which also correlated with a decrease in the BET surface area.

In the first part of this study we present the results of a detailed investigation of the aging and partial deactivation of four chromium exchanged ZSM-5 catalysts during the oxidative destruction of 1% CVOC (vinyl chloride (VC) or trichloroethylene (TCE)) in a humid (1.35% water) air stream at 500°C. Such high feed concentrations and temperatures were used in order to expedite the deactivation process, keeping in mind that the accelerated aging process may not be kinetically identical to the one which obtains at the milder conditions of temperature and concentration which occur commercially. The objective was to show the effects of several factors including the chromium content of the catalyst, the Si/Al ratio of the ZSM-5 support, and the chlorine content of the feed molecule on the deactivation of these catalysts. Over a period of 51 h on stream, all catalysts were found to undergo measurable irreversible deactivation along with the partial loss of catalytically active component, i.e., chromium. Nevertheless, changes in catalyst activity were not entirely correlated by chromium cation content, suggesting that cation location in the pore structure could also be important. A proposed deactivation pathway, involving the slow generation of volatile CrO_2Cl_2, is detailed to explain the process of gradual chromium cation migration within, and loss from, the zeolite matrix.

Catalyst Structure–Activity Relationships

The number and location of active sites in a catalyst are known to determine the catalytic activity (8). The location of active sites becomes especially critical in zeolite catalyst systems since zeolites are made up of crystalline arrays of cages and channels with dimensions close to molecular size, ultimately rendering some or all active sites inaccessible to reactant molecules. Hence, a structural analysis of a given zeolite catalyst to locate actual sites is very useful in understanding its activity.

Using a different cation (Cu), an interesting study by Parrillo *et al.* (9) involving N_2O decomposition over Cu–Y and Cu–ZSM-5 (with similar Si/Al ratios) found that it is the structure of the zeolite (Y- or ZSM-5-) that primarily influences the activity of the catalyst rather than the Si/Al ratio and Cu content. They also showed that the cations exchanged into a Y-zeolite do not remain at tetrahedral sites; instead they tend to migrate to less accessible locations. The original cations residing at the tetrahedral sites are thus replaced by protons, resulting in traditional Brønsted acidity. The openness of the structure of Y-zeolite, compared to that of ZSM-5, was cited as the reason for the migration of cations. Kucherov *et al.* (10) observed that the topography of the isolated Cu^{2+} sites in Cu–ZSM-5 may change after high temperature treatment (steaming at 620°C or calcination at 900°C), resulting in the loss of catalytic activity.

Matsumoto *et al.* (11), in their study of the Cu–ZSM-5 catalysts for lean-NO_x combustion, suggested (based on the evidence from EPR studies) that Cu^{2+} locations change during the reaction, resulting in the deactivation of the catalysts. It was also proposed that the Cu^{2+} ions migrate in the ZSM-5 structure during hydrothermal treatment to positions where they cannot chemisorb NO effectively. Migration of Cu^{2+} ions due to their interaction with reactant molecules (NO) was also hypothesized by Tanabe *et al.* (12), based on their ESR/EPR experiments with the same catalyst system.

Several other studies (13–15) are available in the literature which propose the interaction of metal catalyst cations with reactant molecules in an effort to formulate structure–activity relationships. Surprisingly, there is very little literature available on structure–activity relationships which utilizes data from an X-ray powder diffractometer, a relatively inexpensive and common instrument found in most catalysis laboratories. Instead, researchers (16–19) have utilized data of this type only to elucidate cation locations in catalytic systems without regard to establishing structure–activity correlations.

In the second part of this study, we present cation location, loss, and migration results for the Cr–ZSM-5 oxidation catalysts previously tested. These results are obtained using X-ray powder diffractometer data combined with the Rietveld pattern matching refinement techniques. In combination with the activity, selectivity, and deactivation results already reported herein, these latter efforts allow us to draw conclusions as to the relationships between catalyst crystal structure and catalytic destruction efficiency for CVOC oxidation. The ultimate goal of this study is to improve the design methodology for catalysts capable of resisting deactivation, based on the concept of locating and retaining active catalyst sites in the most accessible and stable locations.

Description of the ZSM-5 Structure

ZSM-5, with its aluminosilicate framework, belongs to the family of pentasil zeolites, but contains considerably less aluminum than a Y-zeolite specimen. ZSM-5 crystallizes in the space group *Pnma* and can have either orthorhombic or monoclinic symmetry (20), which is easily distinguished by the splitting of the ⟨1 3 3⟩ (Miller index) peak. The approximate unit cell parameters are:

$$a = 20.2\ \text{Å} \qquad b = 19.92\ \text{Å} \qquad c = 13.42\ \text{Å}.$$

The unit cell volume ranges from 5345 $Å^3$ to about 5400 $Å^3$ depending on framework aluminum quantity and, in turn, the Si/Al ratio. The unit cell formula for ZSM-5 can be written as $M_xAl_xSi_{96-x}O_{192}$. It has a three-dimensional channel system defined by 10-membered ring openings. The straight channels are parallel to ⟨0 1 0⟩ and have dimensions of

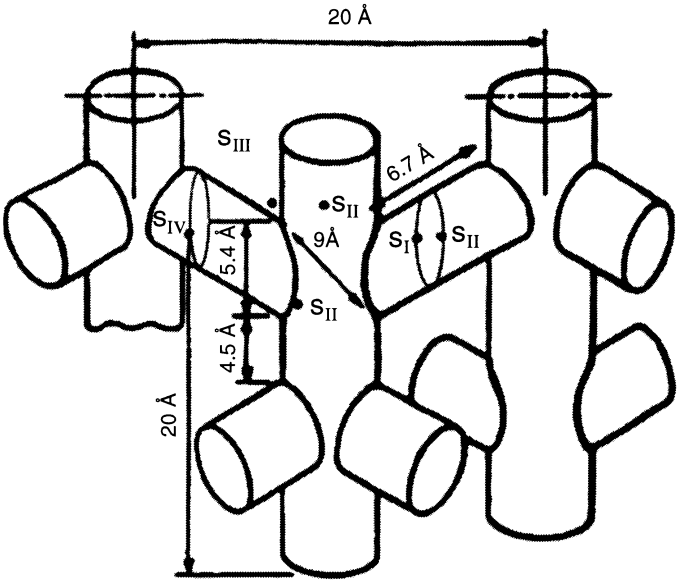

FIG. 1. Cation locations in Cr-ZSM-5; structure from (25).

5.4×5.6 Å, whereas the intersecting sinusoidal channels are parallel to ⟨1 0 0⟩ with pore openings of 5.1×5.5 Å, as shown in Fig. 1.

A unit cell of ZSM-5 consists of the following features (21):

(i) four sinusoidal channels, 5.1×5.5 Å
(ii) four straight channels, 5.4×5.6 Å
(iii) four intersections, 8.7–9.0 Å.

Nomenclature for the exchangeable (charge compensating) cation sites is not as standardized as for faujasites. Consistent with Fig. 1, the nomenclature used in this study for ZSM-5 site locations is listed below:

(a) S_I, midway along the surface of the sinusoidal channels;

(b) S_{II}, within the open straight channel cross section, near the intersections;

(c) S_{III}, subsurface, top and bottom edges of sinusoidal channels, near intersections;

(d) S_{IV}, 2/3 of the way along the surface of the sinusoidal channels.

EXPERIMENTAL

Catalyst Preparation and Testing

Four different chromium exchanged ZSM-5 catalysts, viz., Cr-Z15L, Cr-Z15H, Cr-Z40L, and Cr-Z40H, were used in this study. The numbers 15 and 40 indicate the atomic Si/Al ratios of the ZSM-5-zeolites and suffixes L and H refer to low (∼0.25 wt%) and high (∼0.56 wt%) chromium loading, respectively. The ZSM-5 zeolites contained 20 wt% alumina binder and were obtained from The PQ Corporation in the form of 1/16 in. extrudates. These extrudates were subjected to a single chromium exchange using aqueous $Cr(NO_3)_3 \cdot 9H_2O$ solutions at 80°C for 72 h. In order to obtain the desired chromium loadings, the concentration of precursor solution was adjusted accordingly. The initial pH of the exchanging solution was also adjusted to 4.5 by the addition of a few drops of aqueous NH_4OH. After the exchange, the catalyst extrudates were thoroughly washed with distilled and deionized water, dried, and then calcined at 500°C for 8–10 h.

The aging studies were carried out in a vertical Pyrex tubular reactor (31 mm o.d., 27 mm i.d., and 110 cm length), a schematic of which has been shown elsewhere (22). The reactor had a preheater section for heating the feed gases prior to entering a fixed bed catalyst section where the reactions took place. For all aging experiments, a feed concentration of 1% CVOC (VC or TCE) in humid air (∼1.35% water) was utilized. For VC (b.p. −13°C), a premixed gas mixture (2% in nitrogen, Matheson) was diluted with humid air and fed into the reactor. For TCE, a bubbler maintained at 60°C containing liquid TCE (b.p. 87°C) was used to feed the reactor by passing air through it to vaporize TCE for its passage into the reactor. A separate bubbler containing water was used to humidify the reactor influent.

The aging runs were carried out at 500°C and 1% CVOC concentration in humid air for 51 h at the space velocity of 2400 h^{-1} (measured at RTP). Thermocouples for temperature measurement and control, located at the wall of the reactor, maintained 500°C (±4°C) readings throughout the aging runs. This was aided by automatic cycling of the furnace, which was periodically in the off mode, thus acting as a heat sink to correct for the exothermic nature of the CVOC oxidation reactions. It is likely that a modest radial temperature gradient (not measured) existed within the reactor during high conversion runs of the 1% CVOC feeds. The values of CVOC concentration and temperature used here were considerably more severe than typical remediation conditions (<100 ppm CVOC and ∼350°C) in order to hasten catalyst deactivation.

Catalytic activity and selectivity were measured periodically at 500°C and 1% CVOC and also at 300°C and 1000 ppm CVOC while maintaining the water concentration at ∼1.35%. Data at the lower temperature (300°C) were used to track catalyst activity because conversions uniformly approached 100% at 500°C. Conversely, data at 500°C were used to compare selectivities since differences were most apparent at these conditions.

At the completion of each aging experiment, a combustion test was performed on the catalyst to detect the presence of any residual carbon and/or chlorine-containing species that could have been adsorbed on the catalyst surface during aging. In this test, the feed (CVOC and water) was shut off from the reactor and the catalyst was calcined in flowing air at 550°C for 3 h. During this period, the reactor

effluent was carefully monitored for any residual Cl_2, HCl, CO, or CO_2.

Analysis of the reactor inlet and effluent gas mixtures during the aging studies was performed using a Hewlett Packard 5890 gas chromatograph (GC) with 5970 mass selective detector (MSD). Calibration gas mixtures were periodically injected into the GC/MS to quantify the amounts of CVOCs, CO_2, and other products. Details of the analytical techniques are discussed elsewhere (22).

The fresh and aged catalysts were characterized for their BET surface area (Quantachrome Jr. BET surface area analyzer), chromium content (Phillips PV 9550 X-ray fluorescence spectrometer, XRF), relative crystallinity (Phillips APD 3720 X-ray diffractometer with Cu$K\alpha$ radiation, XRD), and ammonia acidity by temperature programmed desorption to 550°C (DuPont 2950 thermogravimetric analyzer, TPD). The XRF was also used to independently check for the presence of any carbon and/or chlorine-containing species on the surface of aged catalysts.

Catalyst Characterization and Crystal Structure Analysis

Standard mid-range IR analysis (Bio-Rad, Model FT-7) of framework vibrations in the ZSM-5 structure was carried out to document any changes during catalyst aging. XRD patterns of the catalysts were also obtained and the degree of crystallinity was calculated based on the five characteristic peak intensities in the region of 22–25° 2θ. These powder diffraction patterns were used in conjunction with the Rietveld refinement to determine cation locations and occupancy levels. Only the fresh and aged high chromium samples (Cr-Z15H and Cr-Z40H) were considered for the Rietveld analysis since the metal cation content was below calibration limits in the low chromium aged samples. An exception was the Cr-Z40L sample, which was analyzed fresh in order to compare its cation locations with aged catalyst samples of similar chromium content.

The diffraction pattern data collection was repeated to confirm the precision of the instrument as well as to determine any drifts in the sensitivity. The diffraction patterns of as-received H-ZSM-5, were used as the basis for comparison with the other cation-substituted zeolite catalysts. The input file for the Rietveld refinement was prepared by following the standard procedures mentioned in the manual for GSAS (23). The low angle (0–18°) portion of the data was excluded during the refinement procedure to minimize the distortion of relative intensity due to surface roughness and beam spillover (24). Usually, a radial distribution function was chosen to represent the background since this is the preferred method for modeling any amorphous component in the zeolite sample. The initial profile parameter values were taken using refinements carried out with data from a similar diffractometer. The lattice parameters and starting framework coordinates for the ZSM-5 structure were taken from van Koningsveld (25).

ZSM-5 was refined in the orthorhombic *Pnma* space group. There was no splitting of the ⟨1 3 3⟩ peak in the diffraction pattern, which also confirmed that the space group was indeed *Pnma*. All tetrahedral atoms (T-atoms) were treated as Si and were assigned a single isotropic thermal parameter (U_{iso}), and all framework oxygen atoms were constrained to have the same U_{iso}. Typical starting lattice parameter values for ZSM-5 were $a = 20.12$ Å, $b = 19.93$ Å and $c = 13.42$ Å. The framework coordinates of a separate as-received H-ZSM-5 sample were refined and no significant change from these atomic coordinates was observed; hence the framework atoms were fixed for all further work, and not routinely refined.

Initially, only the global parameters such as scale factors, lattice parameters, background and profile coefficients were refined. The shifts to be applied to the refinable parameters in each cycle were heavily damped initially and, as the changes in the parameter values decreased, the damping was decreased. Once the framework structure was stabilized, difference Fourier density maps were calculated to identify any extraframework species. The difference Fourier maps showed uncompensated electron density at positions which were definitely not framework atoms and whose coordinates closely matched with extraframework positions established in the literature. Hence, they were believed to be reasonable, not spurious peaks. Only the peaks with a cation-oxygen bond distance greater than 2.05 Å (called "reasonable peaks") were kept because that is the minimum length of a Cr–O bond. These peaks were added in, one at a time; their atomic coordinates and occupancies, along with the global parameters, were then refined further. This process was continued until no further "reasonable peaks" were left in the difference Fourier map. Although the Cr–O contact distances determined in the samples were longer than a normal Cr–O bond, they were too short to be O–O bond distances between water molecules and framework oxygens. Since there were no other cations present, and since the coordinates found were very similar to those given in the literature (13–15), the evidence supports the conclusion that the nonframework species found was Cr.

At the end of each iteration of refinement, difference plots were drawn which displayed the observed, calculated, and the difference patterns to identify any systematic errors in the structure model. The difference plots also helped to detect the presence of any extra phases in the zeolite sample. The refinement process was stopped when the least square residuals were essentially constant between iterations. It was found from the refinement process that there was, on average, about 3–4% improvement in the final residual values from the time the cations were introduced into the structure to the final refinement cycle. The residuals (R_{wp} and R_p) at the completion of the refinement ranged, respectively, between (14.29 and 10.87% for R_{wp}) and (12.55 and 9.69% for R_p). The bond distances and angles were

computed with the built-in routine in GSAS (23), yielding an average T–O bond distance of about 1.59 Å.

The accuracy and precision of the refinement procedure were confirmed by analyzing the X-ray diffraction data of an Na–Y sample which had been previously published in the literature (24). Very close agreement was found between the refined structure and the published data. This analysis was considered as a measure of the quality of the diffractometer data and the Rietveld method for structure analysis. The three-dimensional structures of the zeolite samples, resulting from refinement results, were visualized with the structure drawing software "XTALDRAW" (26).

RESULTS

Properties of the Fresh Catalysts

Properties of the fresh catalysts are shown in Table 1. Chromium content of the fresh low and high chromium catalysts of this study ranged from 0.23 to 0.57 wt% chromium, respectively. The percentage ion exchange, calculated on the basis of one Cr^{3+} cation for three NH^{4+} cations, varied from 16 to 90%, while BET surface area ranged from 345 to 390 m^2/g. All the fresh catalysts were assigned 100% relative crystallinity (based on XRD) and were used as a reference for the aged catalysts. The total acidity of the catalysts, as measured by the amount of ammonia which was reversibly desorbed, showed that the total acidity was related only to the Si/Al ratio of the ZSM-5 supports and nearly independent of the chromium content of the catalysts. Table 1 also indicates that all the fresh catalysts were capable of nearly complete (>97%) destruction of VC (300°C and 1000 ppm) in humid air. However, under identical reaction conditions, only the fresh high chromium catalysts exhibited >90% destruction efficiency for the TCE feed.

TCE Aging Results

The changes occurring in the activity of the four Cr–ZSM-5 catalysts during prolonged exposure (~51 h) to 1% TCE in humid air at 500°C are depicted in Fig. 2, which shows that, although the catalysts were very active initially, they undergo significant deactivation at these severe conditions. Catalytic activity was strongly dependent on the chromium content of the catalysts, with TCE conversion of Cr–Z40H and Cr–Z15H catalysts always above that of the Cr–Z40L and Cr–Z15L catalysts, respectively, and essentially independent of Si/Al ratio.

The changes in selectivity for deep oxidation products (i.e., CO_2 and Cl_2) during TCE aging at 500°C are also shown in Table 1. Although all the fresh catalysts showed 70–100% selectivity toward the formation of CO_2, selectivity eventually dropped to between 8 and 45% after aging, depending on the Si/Al ratio and chromium content of the zeolite. Similarly, all catalysts showed a progressive reduction in Cl_2 selectivity with time, although high chromium catalysts always had higher CO_2 and Cl_2 selectivities than the low chromium ones. In addition to the unreacted CVOC, CO, CO_2, Cl_2, and HCl in the reactor effluent stream, a small amount (40–70 ppm) of phosgene ($COCl_2$) was also detected with the Cr–Z15H catalyst at 500°C and 1% TCE concentration. Phosgene was not detected with any other catalyst at any conditions. Reactor carbon balances were carried out only for the initial (<1 h) and final (~51 h) sampling points during the aging tests, with values

TABLE 1

Properties of Fresh and Aged Catalysts

Property	Cr–Z15L			Cr–Z15H			Cr–Z40L			Cr–Z40H		
	Fresh	D_{VC}	D_{TCE}	Fresh	D_{VC}	D_{TCE}	Fresh	D_{VC}	D_{TCE}	Fresh	D_{VC}	D_{TCE}
Total acidity (mg NH_3 desorbed/g catalyst)	19.47	19.52	19.48	20.81	19.73	19.73	12.77	13.20	11.90	12.69	11.86	11.99
BET S.A. (m^2/g)	345	329	336	346	342	344	392	405	388	388	407	410
Cr content (wt%)	0.23	0.21	0.12	0.56	0.45	0.21	0.29	0.24	0.16	0.57	0.45	0.33
Relative crystallinity (%)	100	95	97	100	99	100	100	96	103	100	95	103
TCE Conv[a] (%)	64	NA	27	89	NA	54	78	NA	36	93	NA	68
VC Conv[a] (%)	99	95	NA	97	96	NA	98	94	NA	98	95	NA
Cl_2 Sel[b] (%)												
TCE	62	NA	22	75	NA	34	50	NA	18	66	NA	28
VC	4	0	NA	8	4	NA	10	4	NA	10	7	NA
CO_2 Sel[b] (%)												
TCE	66	NA	9	100	NA	43	75	NA	15	100	NA	45
VC	90	63	NA	97	88	NA	90	82	NA	98	94	NA

Note. D_{TCE}, catalyst aged 51 h at 500°C, 1% TCE; D_{VC}, catalyst aged 51 h at 500°C, 1% VC.

[a] At 300°C, 1000 ppm CVOC.

[b] At 500°C, 1% CVOC.

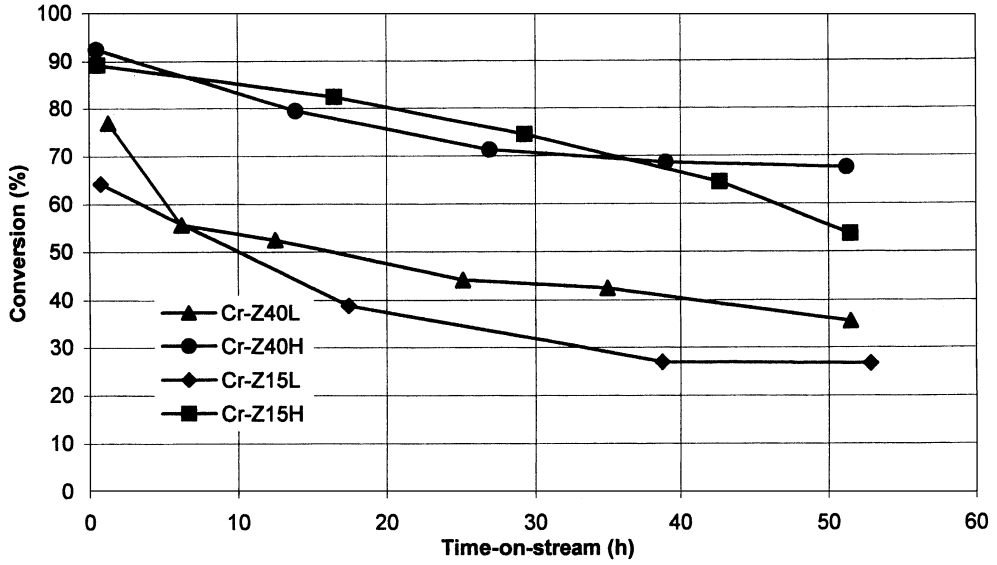

FIG. 2. Activity with time for TCE feed; measured at 1000 ppm TCE in humid air at 300°C and 2400 h^{-1} space velocity. Aging was at 1% TCE and 500°C.

ranging from 93 to 104%. Chlorine balances were not attempted.

VC Aging Results

The effects of prolonged VC exposure on activity of the four catalysts at 500°C and 1% VC concentration in humid air are shown in Fig. 3. As opposed to the significant deactivation observed with TCE, changes during the VC aging were small and extremely slow, and even the aged catalysts showed high (≥93%) conversion. For this reason, no specific trends as a function of the chromium content or the Si/Al ratio of the catalysts could be observed.

Although the activity of the four catalysts did not show much loss during the oxidative destruction of VC, Table 1 shows that the reductions in CO_2 and Cl_2 selectivities (measured at 500°C and 1% VC concentration) were more pronounced. Thus, all the fresh catalysts yielded 90–97% CO_2 selectivity, which eventually dropped to 63–93% after aging. With VC feed, the initial Cl_2 selectivity was very low (≤10%) and gradually reduced to 0–7% after aging.

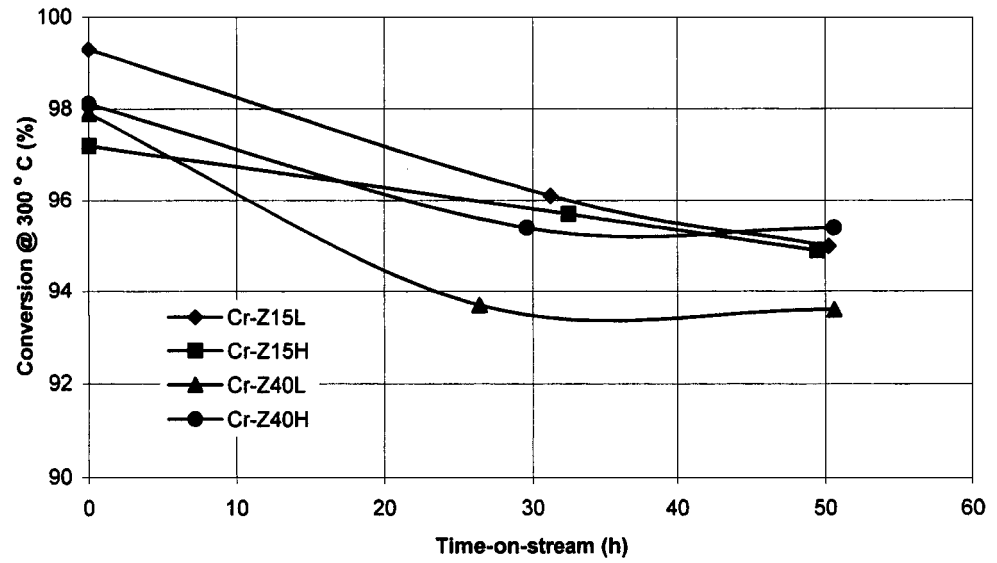

FIG. 3. Catalyst activity with time for VC feed; activity measured at 1000 ppm VC in humid air at 300°C and 2400 h^{-1} space velocity. Aging was at 1% VC and 500°C.

Comparison of Properties of the Fresh and Aged Catalysts

Surface area. Various properties of the fresh and deactivated catalysts are compared in Table 1. As shown there, the BET surface areas of the catalysts did not change significantly upon aging, although zeolite surface area measurements by the BET method are not very precise. The retention of BET surface area also confirms the probable retention of crystal structure after aging.

Crystallinity. The XRD patterns of each catalyst (fresh, VC aged, and TCE aged) were found to be almost identical, indicating no measurable loss of crystallinity upon aging. Although only approximations (27), the relative crystallinities, calculated by comparing the intensities of the identifying reflections (four reflections in the 2θ of 22–25°) of the catalyst and the corresponding reference, are found in Table 1. No new X-ray reflections were found for the aged catalysts, indicating the absence of any crystalline chromium containing species >40 Å (28).

The comparison of the XRD baselines of the three catalysts also indicated the absence of a halo (an increase in the background) after aging. These halos are known to be caused by amorphous material trapped inside the zeolite crystallites (27), and their absence here in the aged catalysts suggests that amorphous species such as silica and silica–alumina were not formed during the deactivation process. Although chromia is crystalline, the size restrictions of zeolite pores will inhibit the internal growth of XRD-detectable (>40 Å) crystalline chromia.

The retention of the ZSM-5 crystal structure is further confirmed by framework FT-IR spectra. According to Flanigen (29), in ZSM-5-zeolite the shift to a higher frequency of the O–T–O band ($T \equiv$ Si, Al) at ~1100 cm^{-1} indicates framework dealumination, and a decrease of the intensity ratio (I_{550}/I_{450}) for the bands at 550 and 450 cm^{-1} indicates crystallinity loss. Neither of the above-mentioned phenomena was found to occur upon aging, further indicating the absence of framework dealumination and the subsequent loss of crystallinity.

Chromium content. As opposed to insignificant changes in the BET surface area and the relative crystallinity, the chromium content (shown in Table 1) dropped 10 to 63% upon aging depending on the choice of the reactant (VC or TCE), with losses being considerably higher for the TCE feed.

Acidity. From Table 1, none of the catalysts used in this study incurred any significant change in ammonia acidity upon aging even though there was a 10 to 63% loss in chromium. This is consistent with FT-IR results, which showed that aging did not change the relative crystallinity or framework aluminum content of any of the catalysts.

Activity. From Table 1, with all the catalysts tested, the VC feed (one Cl atom per molecule) was significantly easier to destroy than the TCE feed (three Cl atoms per molecule). Also, the VC aged catalysts showed <5% loss of their conversion efficiency measured at 300°C and 1000 ppm feed concentration in humid air. Nor did the VC aged catalysts show any trend in catalytic activity as a function of Si/Al ratio, and there is only a slight correlation with initial chromium content. On the contrary, with TCE feed, all catalysts lost substantial deep oxidation activity after aging.

Crystal Structure Analysis

Unit cell parameters, Cr atomic coordinates, and occupancies. Table 2 gives the unit cell parameters, Cr atomic coordinates, and Cr cation site occupancy levels for the fresh and aged Cr–Z15H and 40H catalysts. Data for fresh Cr–Z40L are also shown. Neither the lattice parameters nor the unit cell volume of the catalysts changed significantly due to aging with either VC or TCE although, on average, the unit cell volume of the Cr–Z40-series catalysts was at least 5 $Å^3$ less than that of the Cr–Z15-series.

Rietveld results, which show favored chromium sites and occupancy levels (Cr atoms/unit cell), indicate that S_I, S_{II}, and S_{III} sites (refer to Fig. 1) are preferred in the fresh catalysts, whereas S_I and S_{IV} are preferred in both the VC and the TCE aged ones. Losses in overall chromium occupancy levels determined from Rietveld refinement data were about 20% for VC aging and about 60% with TCE. Although these percentage losses are generally in line with XRF results, absolute chromium levels measured by the two methods differ, with XRF analyses averaging about 20% higher than corresponding Rietveld ones. This offset may have occurred because of the effects of the generally low catalyst chromium level (~0.2–0.6%) on the accuracy of the Rietveld technique.

Chromium cation migration and loss. Figures 4–6 show the top (straight channels) and side (sinusoidal channels) views of the pentasil structures for the fresh and aged Cr–Z40H catalysts and identify the Cr cation positions with respect to the framework coordinates. The framework oxygen atoms, which are closely coordinated to typical Cr cations, have been identified in Fig. 4 only for reference. For the fresh catalysts, Table 2 shows that S_I was the most common site to be occupied, with Cr cations in fresh Cr–Z15H catalyst located at S_I and S_{III} sites, and those in fresh Cr–Z40H located at the S_I and S_{II} positions.

After VC aging, Table 2 shows that the cations were found at S_I and S_{IV} sites in both Cr–Z15H and Cr–Z40H catalysts. The common feature in both these samples was the preferential migration (along with modest chromium loss during the process) of the more abundant cation population (S_{III} in Cr–Z15H and S_{II} in Cr–Z40H) to the S_{IV} site. In addition, some attendant reduction in S_I occupancy levels was also noted, suggesting that Cr cations are able to migrate from these sites also, although at a lower rate.

Table 2 also shows that TCE aging resulted in the substantial loss (40–60%) of chromium cations from the structure

TABLE 2

Unit Cell Parameters, Cr Atomic Coordinates, and Cr Occupancies in Cr–Z15 and Cr–Z40 Catalysts

Site	Cr atomic coordinates			Occupancy/ unit cell
	x	*y*	*z*	
	Cr–Z15H fresh			
	Unit cell parameters: $a = 20.117$, $b = 19.939$, $c = 13.408$ Å, unit cell vol = 5378 Å^3			
S_I	−0.1999	−0.25	−0.0939	0.36
S_{III}	0.1918	−0.055	−0.0783	1.20
	Cr–Z15H TCE aged			
	Unit cell parameters: $a = 20.125$, $b = 19.944$, $c = 13.407$ Å, unit cell vol = 5381 Å^3			
S_I	−0.1984	−0.25	−0.0965	0.72
	Cr–Z15H VC aged			
	Unit cell parameters: $a = 20.120$, $b = 19.932$, $c = 13.398$ Å, unit cell vol = 5373 Å^3			
S_I	−0.183	−0.25	−0.086	0.08
S_{IV}	0.008	0.25	−0.012	1.08
	Cr–Z40H fresh			
	Unit cell parameters: $a = 20.113$, $b = 19.915$, $c = 13.400$ Å, unit cell vol = 5368 Å^3			
S_I	−0.202	−0.25	−0.088	0.92
S_{II}	0.492	−0.047	−0.038	1.53
	Cr–Z40H TCE aged			
	Unit cell parameters: $a = 20.130$, $b = 19.923$, $c = 13.402$ Å, unit cell vol = 5375 Å^3			
S_I	−0.203	−0.25	−0.075	0.82
	Cr–Z40H VC aged			
	Unit cell parameters: $a = 20.120$, $b = 19.919$, $c = 13.397$ Å, unit cell vol = 5369 Å^3			
S_I	−0.199	−0.25	−0.069	0.77
S_{IV}	0.005	0.25	−0.011	1.23
	Cr–Z40L fresh			
	Unit cell parameters: $a = 20.102$, $b = 19.907$, $c = 13.389$ Å, unit cell vol = 5358 Å^3			
S_{II}	0.39472	0.25	−0.07089	0.78

for both the Cr–Z15H and Cr–Z40H catalysts, while the retained chromium ions were located only at the S_I sites in the aged catalysts. For the Cr–Z15H catalyst, S_I occupancy significantly increased with TCE aging. These results indicate a high level of cation mobility, and subsequent cation loss, during TCE exposure.

The chromium–oxygen bond distances of the fresh and aged catalysts are tabulated in Table 3, which shows that the S_I site was most closely associated (i.e. Cr–O bond distances <3.0 Å) with framework oxygens, O(23 and 24), the S_{III} site with O(3, 9, 10, 13, and 14), and the S_{IV} site with O(10, 23, and 26). Most of these oxygen atoms were near the intersections of the straight and sinusoidal channels. Conversely, S_{II} sites are associated with many framework oxygen atoms, but none of the Cr–O distances are less than 3.9 Å, suggesting weaker bonding.

The cation positions in a fresh Cr–Z40L sample were also determined to compare their locations with those of the TCE aged Cr–Z40H sample since the overall Cr cation contents in these two samples were about the same. It can be seen that in the fresh as-prepared Cr–Z40L sample, the Cr cations were found only in the straight channels (S_{II}), while cations remaining in the TCE aged Cr–Z40H sample were located only at S_I.

Crystal Structure–Activity/Selectivity Comparisons

Fresh Cr–Z15H versus fresh Cr–Z40H catalysts. Since it was previously shown (30) that the activity of unexchanged zeolites for destruction of unsaturated two-carbon CVOC feeds is small, the substantial CVOC conversions detected in the present experiments can generally be correlated with the presence of exchanged chromium in these catalysts. Activities of the fresh Cr–Z15H (S_I, S_{III} occupancies, 0.56% total Cr) and Cr–Z40H (S_I, S_{II} occupancies, 0.57% total Cr) catalysts studied here are similar for each respective CVOC feed, suggesting no site location or Si/Al ratio induced effects on conversion level here. Comparison of both Cl_2 and CO_2 selectivities for each respective catalyst again shows no significant differences.

Fresh versus aged Cr–Z15H and Cr–Z40H catalysts. Comparison of the activity of fresh Cr–Z15H (S_I, S_{III}, 0.56% total Cr) versus VC aged Cr–Z15H (S_I, S_{IV}, 0.45% total Cr) and TCE aged Cr–Z15H (S_I, 0.21% total Cr) shows insignificant activity loss (1%) with VC aging, but major loss (39%) with TCE. In contrast, substantial changes (10–70%) in Cl_2 and CO_2 selectivities are apparent after aging with either VC or TCE feed, where both Cl_2 and CO_2 yields decrease,

while HCl and CO correspondingly increase. For Cr–Z40H, activity comparisons of fresh catalyst (S_I, S_{II}, 0.57% total Cr) versus VC aged (S_I, S_{IV}, 0.45% total Cr) and TCE aged (S_I, 0.33% total Cr) shows 4% activity loss with VC and 28% loss with TCE. Changes in selectivity with aging generally follow those for Cr–Z15H with significant loss in Cl_2 and CO_2 selectivity, especially after aging with TCE.

Fresh Cr–Z40L versus aged Cr–Z40H catalysts. Table 1 shows that the TCE activity of fresh Cr–Z40L (78%) is significantly higher than the TCE activity of aged Cr–Z40H (68%), even though chromium content of the latter is one-third less. This is a clear indication that cation location is an important factor in determining catalyst activity.

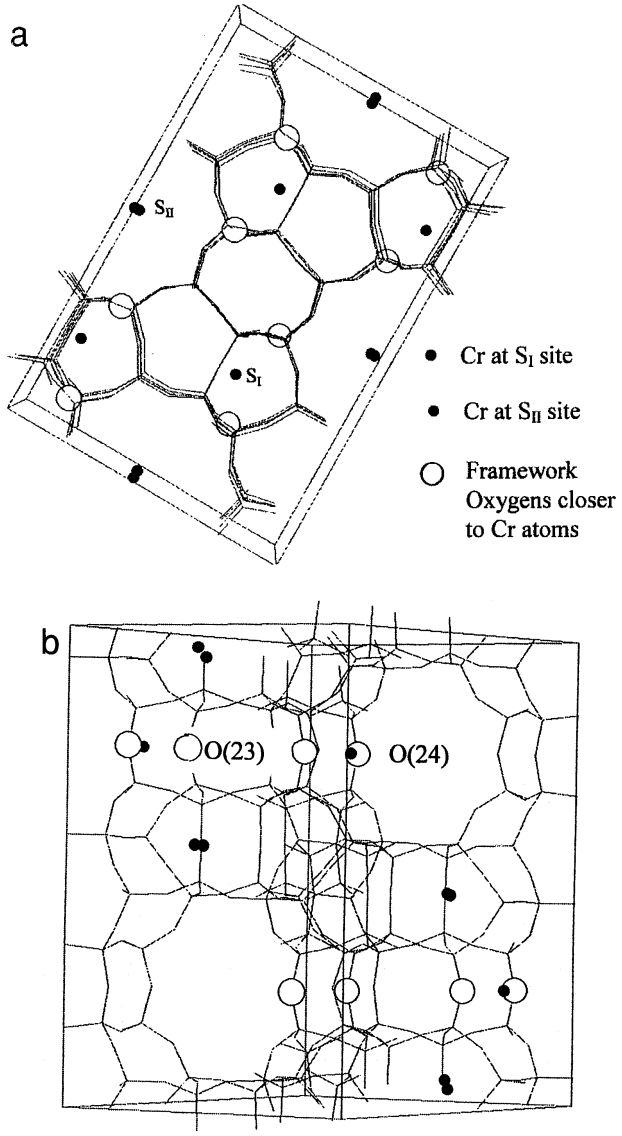

FIG. 4. (a) View down the straight channels of fresh Cr–ZSM5(40H) sample. (b) View of sinusoidal channels of fresh Cr–ZSM5(40H) sample.

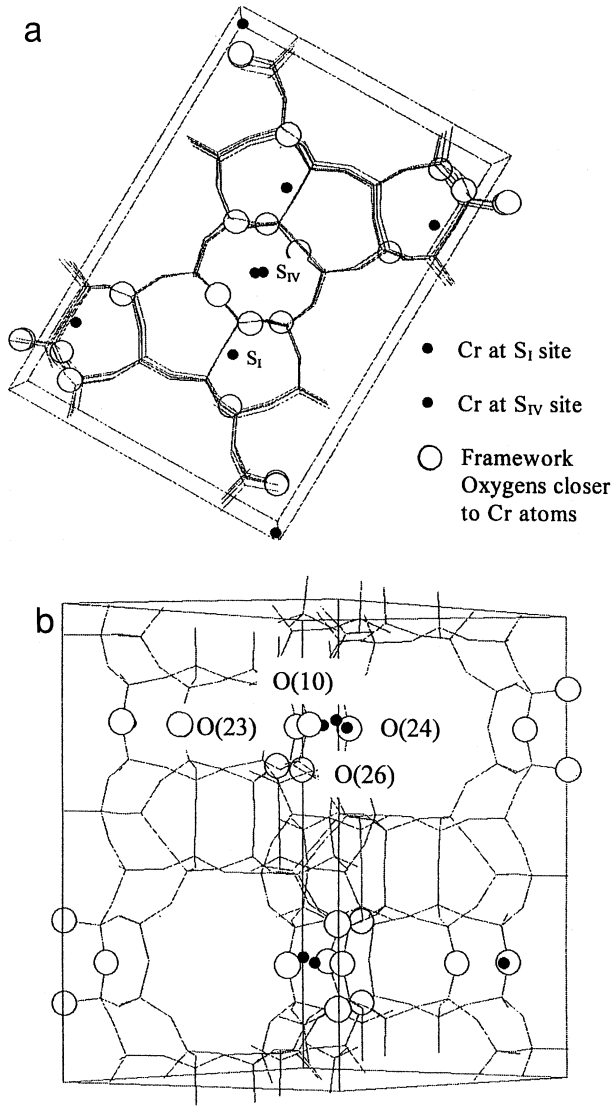

FIG. 5. (a) View down the straight channels of VC aged Cr–ZSM5(40H) sample. (b) View of sinusoidal channels of VC aged Cr–ZSM5(40H) sample.

DISCUSSION

Common Aging Features

Although substantial reductions in deep oxidation activity and selectivity occurred with aging, the crystal structure, framework Al content, surface area, relative crystallinity and total ammonia acidity of the ZSM-5 zeolite remained intact. It should also be pointed out that there was no visible coking, nor did the combustion test (described previously) reveal the presence of any significant carbonaceous or chlorinated species on the catalyst surface. Similarly, the XRF analysis of the deactivated catalysts did not show any detectable chlorine-containing product on the catalyst surface.

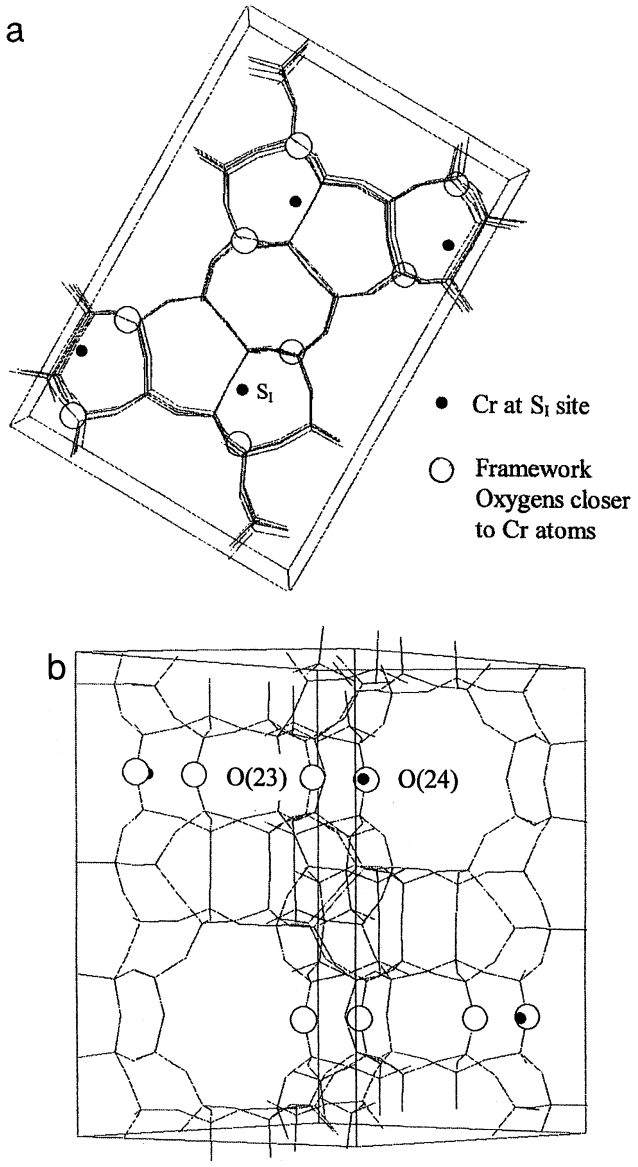

FIG. 6. (a) View down the straight channels of TCE aged Cr–ZSM5(40H) sample. (b) View of sinusoidal channels of TCE aged Cr–ZSM5(40H) sample.

Partial replacement of the zeolitic oxygen and/or hydroxyls by the more electronegative chlorine is considered possible, and a similar phenomenon (replacement of zeolitic oxygen by fluorine) has been observed previously (5). This chlorine/chloride poisoning can lead to the loss of catalytic activity and deep oxidation selectivity (6). However, the replacement of the zeolitic oxygen or hydroxyls by one or more chlorine atoms invariably leads to an increase in the total ammonia acidity, which was not observed in this study.

In fact, the only measured property difference between the fresh and aged catalysts for either CVOC feed was the reduction in chromium content. Nevertheless, chromium content alone cannot explain why fresh Cr–Z40L (0.29% Cr) had significantly higher TCE destruction activity than aged Cr–Z40H (0.33% Cr) as shown in Table 1. This aspect, believed to be related to cation location, is considered subsequently.

Pathways for Catalyst Deactivation

With no significant changes found in catalyst surface area, acidity, or crystallinity after aging, potential pathways for the observed deactivation (other than by chromium loss) are somewhat more limited. It is possible that the documented loss of chromium from the ZSM-5 surface could also be accompanied by other phenomena, such as reduction in cation dispersion (sintering) or by cation migration from site to site within the zeolite matrix. In the discussion that follows, these two possibilities are considered.

Loss of cation dispersion. In the present case, no evidence of chromium oxide species or losses in crystallinity in the aged catalysts were detected by XRD methods. This implies that no crystallites (subject to the >40 Å resolution limit) existed either in the pores or on the exterior zeolite surfaces. Also, the growth of these species in the interior of the zeolite would have required a local structural degradation to accommodate species this large. This would have been reflected in a loss of relative crystallinity, which was not found in any of the aged samples.

Under the humid atmosphere employed in this investigation, it is also possible that water (zeolitic and/or from the feed) reacted with chromium cations forming $Cr(OH)_3$, an electrically neutral species. Being electrically neutral, this species does not require zeolitic protons as anchoring sites and can move along the zeolite channels, aggregating in the form of chromium hydroxide on the external surfaces. Since no such species were detected in the XRD patterns of the aged catalysts, their presence is unlikely.

Cation migration. Next, we consider the possibility that chromium loss was accompanied by its site-to-site migration in the ZSM-5 framework. Although earlier research (31) suggested that for a fixed Si/Al ratio in faujasite catalysts, the CVOC destruction activity of a chromium exchanged zeolite is related only to its chromium content, it is obvious from Table 1 that this is not entirely true for the Cr–ZSM-5 catalysts studied here. For example, as previously mentioned, Cr–Z40H (TCE aged) containing 0.33 wt% chromium shows significantly lower activity than Cr–Z40L (fresh) containing only 0.29 wt% chromium. The same trend can be observed for Cr–Z15H (TCE aged) and Cr–Z15L (fresh) which contain approximately the same amounts of chromium. In each case, the fresh catalysts are more active, even though chromium levels are similar to the aged catalyst values.

These results are consistent with a concomitant process of cation migration during catalyst aging, whereby chromium

TABLE 3

Interatomic Distances (in Å) between Cr and Framework Oxygen Atoms for Cr–Z15H and 40H Samples

	Cr–Z15H fresh	Cr–Z15H VC aged	Cr–Z15H TCE aged	Cr–Z40H fresh	Cr–Z40H VC aged	Cr–Z40H TCE aged
S_I-O(24)	2.30	2.70	2.32	2.29	2.46	2.35
-O(23)	2.58	2.30	2.54	2.64	2.67	2.72
-O(22)	—	4.40	4.65	—	—	—
-O(20)	3.18	3.41	3.2	3.15	3.20	3.14
-O(17)	3.09	2.88	3.08	3.11	3.07	3.12
-O(12)	3.13	3.30	3.12	3.17	3.38	3.30
-O(11)	4.51	—	4.52	4.51	—	4.58
-O(7)	3.32	3.30	3.29	3.39	3.55	3.53
-O(3)	3.89	3.89	3.91	3.88	3.83	3.85
S_{II}-O(22)	—	—	—	3.94	—	—
-O(21)	—	—	—	3.90	—	—
-O(20)	—	—	—	4.48	—	—
-O(19)	—	—	—	4.25	—	—
-O(18)	—	—	—	4.56	—	—
-O(14)	—	—	—	4.25	—	—
-O(13)	—	—	—	4.15	—	—
-O(11)	—	—	—	4.25	—	—
-O(8)	—	—	—	4.30	—	—
-O(7)	—	—	—	4.15	—	—
-O(5)	—	—	—	4.07	—	—
-O(2)	—	—	—	4.30	—	—
-O(1)	—	—	—	4.18	—	—
S_{III}-O(26)	4.61	—	—	—	—	—
-O(19)	3.43	—	—	—	—	—
-O(18)	3.85	—	—	—	—	—
-O(16)	3.21	—	—	—	—	—
-O(15)	3.63	—	—	—	—	—
-O(14)	2.61	—	—	—	—	—
-O(13)	2.74	—	—	—	—	—
-O(12)	3.12	—	—	—	—	—
-O(11)	3.58	—	—	—	—	—
-O(10)	2.98	—	—	—	—	—
-O(9)	2.43	—	—	—	—	—
-O(8)	3.09	—	—	—	—	—
-O(6)	3.27	—	—	—	—	—
-O(5)	3.75	—	—	—	—	—
-O(4)	3.06	—	—	—	—	—
-O(3)	2.71	—	—	—	—	—
-O(2)	3.29	—	—	—	—	—
S_{IV}-O(26)	—	2.47	—	—	2.41	—
-O(23)	—	2.59	—	—	2.62	—
-O(22)	—	3.60	—	—	3.59	—
-O(17)	—	3.20	—	—	3.24	—
-O(15)	—	3.32	—	—	3.29	—
-O(10)	—	2.88	—	—	2.82	—
-O(9)	—	4.55	—	—	4.48	—
-O(4)	—	4.22	—	—	4.25	—

cations move (on balance) to sites which are less accessible to CVOC feed molecules or are otherwise less active. This is in line with results obtained by Matsumoto *et al.* (11) during a study of Cu–ZSM-5 deactivation as previously referenced. In that case, the authors suggested that deactivation was caused by the migration of Cu^{2+} cations to catalytically inactive sites within the ZSM-5.

A plausible process of combined cation migration and loss requires that one or more volatile (i.e., mobile) cation-containing species be formed at the exchanged sites under reaction conditions. These species must then be capable of diffusing within the zeolite pore structure, either recombining with a new surface site (as in the process of chemical vapor deposition, CVD) or leaving the zeolite matrix

entirely. Such pathways are considered in detail in the next section.

Pathways for Chromium Volatilization, Migration, and Loss

Reaction environment. The oxidation of CVOCs (such as TCE and VC) in humid air produces a corrosive environment containing mixed reactants and products. Thus,

$$C_2HCl_3 + O_2 \rightarrow CO_2, CO, HCl, Cl_2,$$

where the amount of chlorine in the feed molecule (TCE = 3 chlorine atoms/molecule; VC = 1 chlorine atom/molecule) has a major influence on catalyst deactivation and exchanged cation loss in zeolites. This strongly suggests the involvement of chlorine-containing products (HCl, Cl_2) with the exchanged chromium sites during deactivation.

State of exchanged chromium sites during CVOC reaction. Data regarding the oxidation state(s) of exchanged Cr cations in ZSM-5-zeolites during reaction with CVOCs in humid air at elevated temperatures are not available, as such, in the literature. However, relevant information from related studies can still be found. Slinkin *et al.* (32) investigated the distribution of Cr^{3+} and Cr^{5+} ions in chromium impregnated ZSM-5 (Si/Al = 20, 0.8–1.8 wt% chromium) under oxygen-rich conditions from 140 to 500°C. Their results suggest that a rise in temperature from 140 to 500°C is followed by an increase in the concentration of Cr^{5+} cations. The authors also state that the concentration of such species depends on the total chromium content of the zeolite.

Previous work by Aparicio *et al.* (33) with chromium exchanged Y-zeolites (Si/Al = 3.4), using methods of magnetic susceptibility and Mossbauer spectroscopy, showed chromium to be primarily in the +5 valence state after oxidation with dry O_2 at 423°C. Extensive studies by Wichterlova *et al.* (34), using IR and ESR techniques with oxygenated Cr–Y (Si/Al = 2.2), showed the presence of both Cr^{+5} and Cr^{+6}, with the concentration of the latter valence state rapidly increasing as temperature approached 497°C. This was thought to be caused by involvement of the chromium with extralattice ligands (primarily oxygen) to form cation bonds of differing strength. The authors point out that *in vacuo* methods, necessary with XPS and ESCA techniques, are marginal here because the highly oxygenated cations (especially Cr^{+6}, which is very unstable) are partially reduced under these conditions. However, under CVOC oxidation reaction conditions (and particularly above 400°C), chromium is known (34) to function in a typical redox fashion by first chemisorbing oxygen to achieve high (+5 or +6) oxidation states. It then interacts with CVOC molecules to bring about momentary reduction (typically to Cr^{+3}), before subsequent reoxidation to the +5 or +6 state.

Based on the electron withdrawing effects of the extra-framework chemisorbed oxygen atoms associated with the chromium cations, it follows that the Cr-to-framework oxygen bonds will be most weakened at the highest cation oxidation state (Cr^{+6}). This situation is shown schematically below:

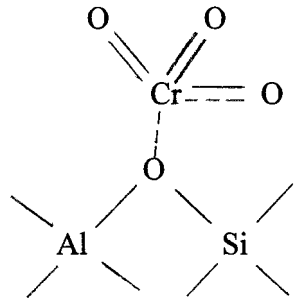

In reality, the chromium cation is most probably coordinated with several closely spaced framework oxygen sites (34), but is shown here with single site involvement for simplicity. Alternately, under the humid conditions considered presently, the Cr-site may also be partially hydrated/hydrolyzed.

The oxygenated chromium cation, with weakened Cr–O framework bond, may be viewed here as a CrO_3-like compound. Under these conditions (500°C in the present study), and in the presence of large concentrations of CVOC reaction products (HCl/Cl_2), the potential for chromium loss becomes significant.

Reaction/volatilization of exchanged chromium cations. Interaction of potentially labile oxygenated chromium cations (i.e., the CrO_3-like compound) with chlorine-containing species is suggested to occur by one or more of the following reactions:

$$CrO_3(s) + 2HCl(g) \rightarrow CrO_2Cl_2(g) + H_2O(g)$$

$$CrO_3(s) + Cl_2(g) \rightarrow CrO_2Cl_2(g) + 1/2\,O_2$$

$$CrO_3(s) + C_2HCl_3(g) + 1/2\,O_2 \rightarrow CrO_2Cl_2(g) + HCl(g) + 2CO.$$

These reactions are listed in order of decreasing probability based on ΔGs, which range from about –60 to –40 kJ at 500°C. In addition, the reversible Deacon reaction,

$$2Cl_2 + 2H_2O \leftrightarrow 4HCl + O_2,$$

favored to the right under humid conditions found in this study, acts to further reduce Cl_2 concentration and therefore the likelihood of the second reaction between CrO_3 and Cl_2.

The primary product, CrO_2Cl_2, is volatile (m.p. = −96.5°C, b.p. = 117°C) at reaction conditions and thus

becomes the likely vehicle for chromium cation mobility and loss. Formation of this same product has been previously suggested by others (6, 35) for involvement in the process of cation loss. Furthermore, CrO_2Cl_2 has been successfully used (36) in the vapor state for chemical vapor deposition of chromium in zeolites.

The maximum chromium loss observed in this investigation during catalyst aging was 0.0035 g chromium/g catalyst (62% loss) from Cr–Z15H catalyst exposed to TCE feed. This loss, under the deactivation conditions used in this study (500 cm^3/min total flow rate and 51 h time-on-stream), would correspond to a steady CrO_2Cl_2 concentration of less than 5 ppm in the effluent stream of the reactor, too low to be detected by our analytical techniques. Furthermore, it is probable that much of the CrO_2Cl_2 lost from the zeolite matrix would have decomposed in the cooler portions of the reactor according to

$$2CrO_2Cl_2(g) \rightarrow Cr_2O_3(s) + 2Cl_2 + 1/2\,O_2,$$

which is thermodynamically favored ($\Delta G = -54.7$ kJ/mol at 25°C). This is consistent with our observation of dark green residues (believed to be Cr_2O_3) after the reaction section, especially during the TCE aging experiments. It is also in line with conclusions drawn by Manning (35) and Agarwal and coworkers (37), who studied the oxidation of CVOCs such as perchloroethylene using Cr_2O_3 impregnated Al_2O_3 catalyst.

Migration and interaction of CrO_2Cl_2 with zeolite sites. Using the scheme proposed by Whittington *et al.* (36), vapor phase CrO_2Cl_2 may interact with unexchanged zeolite sites in the presence of oxygen as follows:

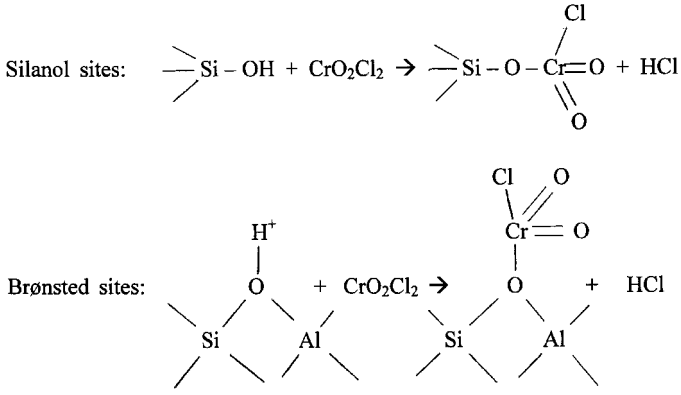

Hydrolysis of the Cr–Cl bonds, under the humid conditions present here during reaction, will subsequently introduce acidic Cr–OH groups at the sites and liberate additional HCl.

In this fashion, the chromium cation is able to migrate to sites of greater or lesser accessibility, strength, or activity within the zeolite matrix. However, Cr sites of greatest accessibility are speculated to be the most vulnerable to later cation revolatilization, suggesting a process of gradual cation retreat in the ZSM-5 structure to locations of high framework bond strength and/or low reactant accessibility.

Crystal Structure Analysis

Fresh catalysts. Comparison of sites occupied by chromium in fresh Cr–Z15H versus fresh Cr–Z40H shows that both catalysts have significant cation occupancies in the S_I position. However, for Cr–Z15H (one Al per 15 Si atoms) primary chromium occupancy is in the S_{III} position, while for Cr–Z40H (one Al per 40 Si atoms) primary chromium occupancy is in the S_{II} position. If we analyze these differences based on site accessibility, site availability, and site strength (as measured by Cr–O bond lengths), it is noted that Cr–Z40H has only 37.5% as many total aluminum atoms (and hence Brønsted sites) per unit cell as Cr–Z15H. Since both catalysts contain similar total Cr levels (~0.56%), a higher overall exchange level in Cr–Z40H is expected.

In terms of close association with framework oxygen atoms, Table 2 shows S_I, S_{III}, and S_{IV} (roughly in that order) to be the chromium sites most closely bound to oxygen atoms, while S_{II} is a distant fourth. If it is hypothesized that the lower overall site population expected in Cr–Z40H, required because of its lower Al atom population, occurs largely from the absence of S_{III} sites, then the chromium occupancy results for these catalysts are consistent with the following criteria: site accessibility (S_{II} and S_{III} are near intersections and/or are in the highly accessible straight channels); site availability (overall, sites are nearly three times more plentiful, especially S_{III}, in Cr–Z15H); cation-to-framework oxygen bond strengths (short bond lengths, as in S_I, imply strength). We see that the low chromium, low aluminum catalyst (Cr–Z40L) is also consistent with these criteria by showing chromium occupancy only at the available, highly accessible, but relatively weak S_{II} sites. In fact, S_{II} Cr occupancy occurs only in the Cr–Z40 samples (H and L), suggesting that the high Si/Al ratio, rather than total Cr level, controls filling of these weak sites.

Aged catalysts. As previously pointed out, the interaction of the chromium cations with products of CVOC oxidation (HCl, Cl_2) causes loss and migration of chromium through the formation of volatile CrO_2Cl_2 and presents a likely mechanism for deactivation of these catalysts. Cation migration in zeolites has already been noted and also discussed elsewhere in the literature (10–14). We reexamine this mechanism and our deactivation results in terms of the previously mentioned occupancy criteria (site accessibility, site availability, and Cr–O bond strengths). In addition we also take into account the nature of the CVOC, and its potential for producing HCl and Cl_2 during oxidation.

Results show that aging with TCE (3 Cls per CVOC molecule) consistently causes major loss of Cr (42–63%) and also major shifts in site occupancy by cation migration

in the catalysts. Conversely, aging with VC (1 Cl per CVOC molecule) causes only minor loss of Cr (20–21%); however, significant shifts in site occupancy to the less accessible sinusoidal channels are evident. These results are consistent with the deactivation mechanism just discussed, whereby interaction of the oxygenated Cr sites with reaction products (HCl and Cl_2) causes mobility of the cation by formation of CrO_2Cl_2. The higher halogen concentration present during oxidation of TCE can be expected to translate into higher local concentrations of CrO_2Cl_2, facilitating its loss by diffusion from the zeolite matrix.

Regardless of CVOC feed or zeolite Si/Al ratio, the results show that Cr migration during aging is always from accessible sites (S_{II}, S_{III}) in the straight channels or in the intersection region, to less accessible sites (S_I, S_{IV}) in the sinusoidal channels. It is probable that Cr loss occurs most rapidly from the S_{II} sites (only occupied at all in the high Si/Al catalyst) since it is both highly accessible to halogenated products within the straight channels, and also relatively weakly bound to the framework oxygen atoms of the zeolite. Conversely, Cr which eventually migrates to (or which is initially exchanged with) the less accessible sites in the sinusoidal channels (S_I, S_{IV}) is bound more strongly and hence is more resistant to halogen attack.

Crystal Structure–Activity/Selectivity Comparisons

Fresh Cr–Z15H versus fresh Cr–Z40H catalysts. The similarity in CVOC activity and selectivity for these two catalysts, in spite of S_I, S_{III} Cr occupancy for Cr-Z15H versus S_I, S_{II} Cr occupancy for Cr–Z40H, suggests that CVOC accessibility to S_{III} compared with S_{II} sites in these fresh catalysts is roughly equivalent. This result appears logical since both sites are located in the straight channel/intersection regions of the zeolite structure, which have maximum access to incoming CVOC feed molecules.

Fresh versus aged Cr–Z15H and Cr–Z40H catalysts. The lower Cr loss for Cr–Z40H during aging is consistent with the notion of greater site strength in zeolites as sites are moved farther apart. This is in agreement with our NH_3-TPD results which showed higher temperatures necessary for complete NH_3 desorption, implying a population containing a number of stronger sites with the Cr–Z40H catalyst. This is also consistent with the unit cell formula for ZSM-type zeolites ($Al_nSi_{96-n}O_{192}$) which predicts 6 Al atoms per unit cell for Si/Al = 15 and only 2.3 for Si/Al = 40.

The lower Cr loss from TCE aging of the high Si/Al ratio catalyst may also be primarily responsible for the smaller reductions in activity (but nearly equivalent changes in selectivity) after aging, between Cr–Z40H and Cr–Z15H. This seems most plausible, because the Cr migration process during aging appears very similar for the two different Si/Al ratio catalysts. In both cases the migration process leaves Cr in the S_I position after TCE aging and in the S_I and S_{IV} positions after VC aging. Since Cr site locations after aging are identical for the two catalysts, CVOC accessibility to these sites as an explanation for differences in catalyst activity must be ruled out in this case.

Fresh Cr–Z40L versus aged Cr–Z40H. The difference in TCE activity between these two catalysts (78% for fresh Cr–Z40L versus 68% for aged Cr–Z40H) is significant, particularly in light of the fact that the lower activity catalyst (aged Cr–Z40H) still contains almost 50% more Cr than does the more active fresh Cr–Z40L catalyst. The difference in catalyst activity in this case appears to trace directly to variations in cation location (and hence CVOC accessibility) in the two catalysts. All Cr cations in the fresh Cr–Z40L are located in the highly accessible, but weakly anchored S_{II} sites. One would expect an active, but unstable, catalyst in this case as compared to aged Cr–Z40H, where (even with higher chromium level) the overall CVOC accessibility of the S_I sites in the sinusoidal channels is lower. Conversely, the S_I sites should be more stable, based on Cr–O bond lengths, and hence catalyst activity for the aged Cr–Z40H might be expected to persist much longer during any subsequent aging process as compared to the fresh Cr–Z40L catalyst. In addition, selectivity to Cl_2 and CO_2 is higher for the fresh Cr–Z40L catalyst, suggesting that cation location (S_{II} versus S_I) and its accessibility to both CVOC and oxygen encourages formation of these more desirable end products.

ACKNOWLEDGMENTS

Partial funding for this research was obtained from the U.S. Environmental Protection Agency, the U.S. Air Force, and SERDP and is acknowledged with appreciation. Special thanks are due Dr. James A. Kaduk (Amoco Corp.) for help in zeolite structure analysis. The authors also thank Dr. Thomas Hastings (The PQ Corporation) for providing the zeolite samples, Mr. Thomas Quick (The University of Akron) for collecting the X-ray diffraction data, and Mr. Troy Semelsberger (Case Western Reserve University) for assistance in graphics and calculations.

REFERENCES

1. Chatterjee, S., Greene, H. L., and Park, Y. J., *J. Catal.* **138**, 179 (1992).
2. Chintawar, P. S., and Greene, H. L., *Appl. Catal. B* **13**, 81 (1997).
3. Rachapudi, R., MS thesis, The Univ. of Akron, 1993.
4. Chatterjee, S., Greene, H. L., and Park, Y. J., *Catal. Today* **11**, 569 (1992).
5. Karmakar, S., and Greene, H. L., *J. Catal.* **148**, 524 (1994).
6. Spivey, J. J., and Butt, J. B., *Catal. Today* **11**, 465 (1992).
7. Agarwal, S. K., and Spivey, J. J., *Appl. Catal. A* **81**, 239 (1992).
8. Gates, B. C., "Catalytic Chemistry." Wiley, New York, 1992.
9. Parillo, D. J., Fortney, J. P., and Gorte, R. J., *J. Catal.* **153**, 190 (1995).
10. Kucherov, A. V., Hubbard, C. P., and Shelef, M., *J. Catal.* **157**, 603 (1995).
11. Matsumoto, S., Yokota, K., Doi, H., Kimura, M., Sekizawa, K., and Kasahara, S., *Catal. Today* **22**, 1127 (1994).
12. Tanabe, T., Iijima, T., Koiwai, A., Mizuuo, J., Yokota, K., and Isogai, A., *Appl. Catal. B* **6**, 145 (1995).

13. Descorme, C., Gelin, P., Primet, M., Lecuyer, C., and Saint-Just, J., "Zeolites: A Refined Tool for Designing Catalytic Sites" (L. Bonnevoit and S. Kaliaguine, Eds.), p. 287. Elsevier, Amsterdam, 1995.
14. Yan, J. Y., Lei, G. D., Sachtler, W. H., and Kung, H. H., *J. Catal.* **161**, 43 (1996).
15. Yu, J. S., and Kevan, L., *J. Phys. Chem.* **94**, 7612 (1990).
16. Huddersman, K., and Rees, L. V. C., *Zeolites* **11**, 270 (1991).
17. Zhenyi, L., Wangjin, Z., Qiu, Y., and Guanglie, L., "Proceedings of 7th International Zeolite Conference" (Y. Murakami, A. Iijima, and J. M. Ward, Eds.), p. 415. Kodansha, Elsevier, Tokyo, 1986.
18. Lin, J. C., Chao, K. J., and Wang, Y., *Zeolites* **11**, 376 (1991).
19. Attfield, M. P., Weigel, S. J., and Cheetam, A. K., *J. Catal.* **170**, 227 (1997).
20. Olson, D. H., Kokatalio, G. T., Lawton, S. L., and Meier, W. M., *J. Phys. Chem.* **85**, 2238 (1981).
21. Richards, R., and Rees, L. V. C., *Langmuir* **3**, 335 (1987).
22. Karmakar, S., and Greene, H. L., *J. Catal.* **138**, 364 (1992).
23. Larson, A. S., and Von Dreele, R. B., "GSAS, The Generalized Structure Analysis System." Los Alamos National Laboratory, November 1994.
24. Kaduk, J. A., and Faber, J., *Rigaku J.* **12**(2), (1995).
25. (a) van Koningsveld, H., van Bekkum, H., and Jansen, J. C., *Acta Crystallogr.* **B43**, 127 (1987); (b) van Koningsveld, H., *Acta Crystallogr.* **B46**, 731 (1990).
26. Downs, B., and Bartlemehs, K., "XTALDRAW." Univ. of Texas at Austin, October 1995.
27. Kharas, K. C. C., Robota, H. J., and Liu, D. J., *Appl. Catal. B* **2**, 225 (1993).
28. Yan, J. Y., Lei, G. D., Sachtler, W. H., and Kung, H. H., *J. Catal.* **161**, 43 (1996).
29. Flanigen, M., *Adv. Chem. Ser.* **121**, 119 (1973).
30. Chatterjee, S., Ph.D. dissertation, The Univ. of Akron, 1994.
31. Chatterjee, S., and Greene, H. L., *Appl. Catal. A* **98**, 139 (1993).
32. Slinkin, A. A., Kucherov, A. V., Gorjachenko, S. S., Aleshin, E. G., and Slovetskaja, K. I., *Zeolites* **10**, 111 (1990).
33. Aparicio, L. M., Ulla, M. A., Millman, W. S., and Dumesic, J. A., *J. Catal.* **110**, 330 (1988).
34. Wichterlova, B., Tvaruzkova, Z., and Novakova, J., *J. Chem. Soc. Faraday Trans. I* **79**, 1573 (1983).
35. Manning, P., *Hazard. Waste* **1**, 41 (1984).
36. Whittington, B. I., and Anderson, J. R., *J. Phys. Chem.* **95**, 3306 (1991).
37. Agarwal, S. K., Spivey, J. J., and Butt, J. B., *Appl. Catal. A* **82**, 259 (1992).